Available online at www.sciencedirect.com
ScienceDirect
Trans. Nonferrous Met. Soc. China 32(2022) 935−946
Transactions of Nonferrous Metals Society of China
www.tnmsc.cn

Fabrication of $MoSi_2$ coatings on molybdenum and its high-temperature anti-oxidation properties

Lu ZHU[1,2], Peng CHEN[1], Zi-ming CAI[1], Pei-zhong FENG[1], Xue-qin KANG[1], Farid AKHTAR[3], Xiao-hong WANG[1]

1. School of Materials Science and Physics, China University of Mining and Technology, Xuzhou 221116, China;
2. School of Chemical Engineering and Technology, China University of Mining and Technology, Xuzhou 221116, China;
3. Division of Materials Science, Luleå University of Technology, Luleå 97187, Sweden

Received 1 March 2021; accepted 26 October 2021

Abstract: Industrial spent $MoSi_2$-based materials were used to fabricate oxidation-resistant coatings on molybdenum via slurry painting in air. The microstructure, phase constituent and high-temperature oxidation behaviors of the coatings at 1500 °C were explored. The results show that the bonding layer is generated in the coatings after sintering, which strengthens the metallurgical combination between the coating and the substrate because of the formation of diffusion layers. Rare cracks appear in the coating using pure $MoSi_2$ (PM coating) while the coating using spent $MoSi_2$ (SM coating) is free of cracks due to decreased thermal expansion mismatch. After oxidation, the oxide scale of PM coating possesses large-sized pores while a relatively dense oxide scale is acquired by SM coating. Compared with PM coating, thinner glassy oxide scale with lower mass gain is obtained by SM coating, exhibiting better anti-oxidation properties at 1500 °C.

Key words: recycling; spent $MoSi_2$; slurry painting; anti-oxidation properties; molybdenum substrate

1 Introduction

As one of the most favored refractory metals, molybdenum (Mo) has a high melting temperature (2620 °C), excellent thermal conductivity and high elastic modulus [1−3]. Therefore, it has been widely applied in the key parts of cannon barrels, rocket engines and nuclear reactors [2−4]. However, when temperature reaches 400−750 °C, Mo will be rapidly oxidized to MoO_3 in air. The volatilization of MoO_3 can cause the rapid invalidation of Mo, which seriously restricts its application at elevated temperature [4].

Fabricating a coating on the surface can effectively extend the lifespan of the substrate without diminishing its properties [5,6]. Lots of coatings, especially silicide coating represented by $MoSi_2$, have been widely researched due to the low density (6.24 g/cm³), high melting point (2030 °C), good thermal conductivity and high working temperature (≤1850 °C) [7,8]. When the temperature is over 1000 °C, a layer of silica can be generated on $MoSi_2$ to prevent further oxidation [9], and consequently $MoSi_2$-based materials are widely used in the high-temperature fields [10].

However, the consumption of $MoSi_2$-based materials increases gradually, and an enormous number of spent $MoSi_2$-based materials are discarded after long-term use in the high-temperature environments, causing environmental pollution and waste of resource. It is worth mentioning that the development of sustainable resources for positive societal, environmental, and

Corresponding author: Zi-ming CAI, Tel: +86-18811328677, E-mail: zmcai@cumt.edu.cn;
Xiao-hong WANG, Tel: +86-13952189920, E-mail: wxhcumt@cumt.edu.cn
DOI: 10.1016/S1003-6326(22)65844-8

economic impacts can be effectively driven by achieving increased utilization of wastes [11]. Although the $MoSi_2$-based materials fail after long-term service, there is no change in its major compositions ($MoSi_2$), indicating that spent $MoSi_2$-based materials still possess excellent anti-oxidation properties. In consideration of the advantages of molybdenum disilicide, spent $MoSi_2$-based materials can be recycled as raw materials to fabricate coating on Mo substrate for potential high-temperature protection.

Although lots of coatings are sintered in a vacuum or protective atmosphere (such as argon) to avoid oxidation [12], it is found that the coating preparation can be accomplished in air by fabricating multilayer structures with pressureless sintering, which is easily operated on various shapes and sizes objects [13]. Without the protective atmosphere, cost for the coating sintering can be significantly reduced. The silica layer, which is formed on the surface of the silicide coating during sintering in the air, can inhibit the further diffusion of O_2, making tiny amounts of oxidation. Furthermore, slurry painting is a simple method to prepare the coating in the air with relatively low requirements of devices [14]. Therefore, it is meaningful to prepare $MoSi_2$ anti-oxidation coating on Mo substrate by slurry painting.

Herein, spent $MoSi_2$-based materials were used as raw materials, and slurry painting was applied to prepare $MoSi_2$ multilayer coating (SM coating) on Mo substrate. For comparative analysis, pure $MoSi_2$ powders were also used to fabricate the coating (PM coating). After sintering at high temperatures, the microstructural evolution of PM and SM coatings were investigated, and the oxidation behaviors of the multilayer coatings at 1500 °C were studied.

2 Experimental

2.1 Coating fabrication

Molybdenum (12.0 mm in diameter, 2.5 mm in thickness, Qinghe Guantai Metal Material Co., Ltd., China) substrate was polished by 1000 grit SiC abrasive paper to remove the grease and impurities from the surface. Industrial spent $MoSi_2$-based materials (Zhengzhou Juding High Temperature Furnace Technology Co., Ltd., China) were sourced from the electrical furnace that worked at 1000−1700 °C for over 1000 h, and used as coating materials after being crushed into powders. The SEM images and corresponding distribution of the spent $MoSi_2$ powders are illustrated in Figs. 1(a−c). The size of powders roughly ranges from 0 to 30 μm, and they were found to be made up of Si, Mo, Al and O elements in the previous study [15].

Firstly, 5 wt.% bentonite solution (Xinjiang Haotai Huamei Mining Technology Co., Ltd., China), in which the solvent was deionized water, was mixed with Si (99.9% in purity, 5 μm, Beijing Wodetai Technology Co., Ltd., China) and spent $MoSi_2$ powders (mass ratio of 5:1:4) to prepare coating slurry to brush Mo substrate as bonding

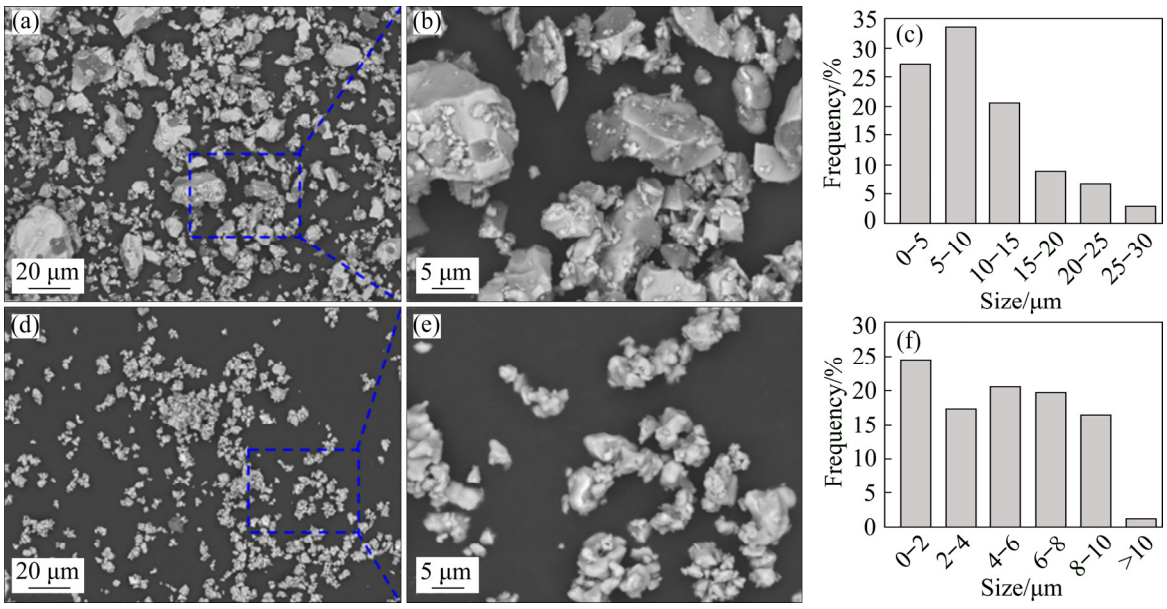

Fig. 1 SEM images and corresponding distribution of spent $MoSi_2$ (a−c) and pure $MoSi_2$ (d−f) powders

layer (Layer I). The main compositions of the bentonite were SiO_2 (71.7 wt.%), Al_2O_3 (16.2 wt.%), Na_2O (3.1 wt.%) and CaO (2.4 wt.%). The bonding between the coating and substrate could be enhanced by the diffusion of Si with Mo, which forms a diffusion layer at elevated temperatures. Secondly, spent $MoSi_2$ powders were added into 5 wt.% bentonite solution (mass ratio of 1:1) to brush Layer I as the protecting layer (Layer II) and it acted as the main part of the multilayer coating to protect the Mo substrate. Thirdly, spent $MoSi_2$, Si powders and glass powders (99.5% in purity, 6.0−11.0 μm, Guangzhou Anywhere New Materials Co., Ltd., China) were mixed in 5 wt.% bentonite solution (mass ratio of 3:1:1:4) to brush Layer II as oxygen-barrier layer (Layer III), which was prepared for the formation of liquid SiO_2 to inhibit the diffusion of oxygen at elevated temperature. The glass powders mainly consisted of SiO_2 (60.48 wt.%) and CaO (25.95 wt.%) by X-ray fluorescence spectrometer (XRF) in Table 1. The glass powders had a low melting temperature (1050 °C) and they were conducive to improving the coating compactness during sintering. Furthermore, SiO_2 in the glass powders could enhance the anti-oxidation properties of the coating at high temperatures. For comparison, multilayer $MoSi_2$ coating was also prepared by commercially pure $MoSi_2$ powders (99.0% in purity, Yantai Torch Special High Temperature Ceramics Co., Ltd., China) under the same technological conditions. The SEM images of the pure $MoSi_2$ powders are shown in Figs. 1(d, e), and its size ranged from 0 to 10 μm, as shown in Fig. 1(f).

After being painted, the coating samples were dried at 60 °C for 24 h, and then were placed into Al_2O_3 crucible. ZrO_2 particles (1−3 mm) were put in the bottom of the crucible to prevent the adhesion of coating samples with crucible during high-temperature sintering. The pressureless sintering of the coating samples was carried out in the electrical furnace without a protective atmosphere and the heating rate was 10 °C/min. Before being cooled to room temperature (RT), the coating samples were held for 1 h as the temperature rose to 1100 and 1400 °C, respectively. Corresponding preparation process of the multilayer coatings is provided in Fig. 2.

Table 1 Chemical composition of glass powders by XRF (wt.%)

SiO_2	CaO	Al_2O_3	BaO	Na_2O
60.48	25.95	5.21	3.15	2.90
K_2O	Sb_2O_3	MgO	ZrO_2	Others
1.15	0.76	0.19	0.09	0.12

2.2 Oxidation test and characterizations

Coating samples were put into the Al_2O_3 crucible and the oxidation tests (1500 °C) of PM and SM coatings were performed in the electrical furnace (0−20 h). After an oxidation test, the coating samples were taken out and then cooled to RT. An electronic balance was used to calculate the mass change of the coating samples (Δm_{cs}):

$$\Delta m_{cs}=(m_a-m_b)/A_{cs} \quad (1)$$

where m_a and m_b are the masses after and before oxidation, respectively, and A_{cs} is the surface area of the coating samples before oxidation test.

Scanning electron microscopy (SEM, JEOL JSM−IT300LV) with energy dispersive spectroscopy (EDS) was used to observe microstructure of the powders and coatings, and the phase composition of PM and SM coatings was detected by X-ray diffraction (XRD, Panalytical Empyrean). The chemical composition of the glass powders was tested by X-ray fluorescence spectrometer (XRF,

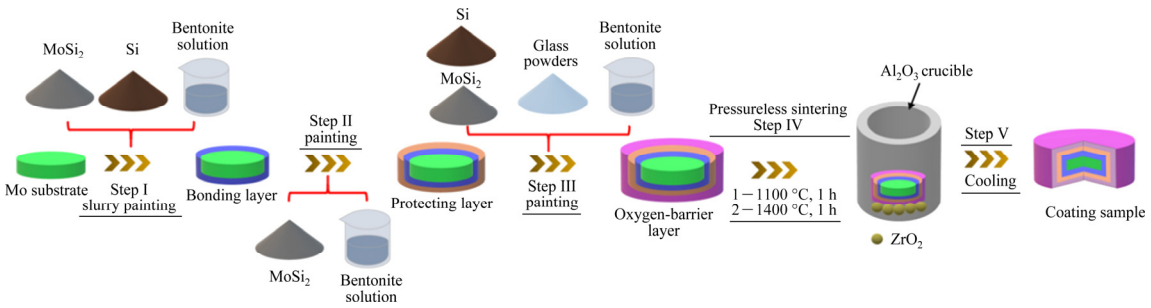

Fig. 2 Schematic illustration of preparation process for multilayer coating by slurry painting

Thermo Fisher 9900). Transmission electron microscopy (TEM, JEM−3010) was used to analyze the micromorphology of spent $MoSi_2$ powders.

3 Results and discussion

3.1 Phase and microstructure

Figure 3 shows the XRD patterns of pure $MoSi_2$ and spent $MoSi_2$ powders. $MoSi_2$ has high intensity in the XRD patterns of the pure and spent $MoSi_2$ powders, and Mo_5Si_3 phase with relatively weak intensity can be observed in the spent powders since Mo_5Si_3 and SiO_2 phases are generated in the $MoSi_2$-based materials after long-term service at elevated temperature. Based on our previous research [15], the spent powders consist of Mo (60.17 wt.%) and Si (33.62 wt.%) with rare amounts of O (3.09 wt.%), Al (1.76 wt.%), Ca (0.11 wt.%), etc. However, owing to the low content and amorphous state of the SiO_2 phase, it is difficult to be detected in the XRD patterns.

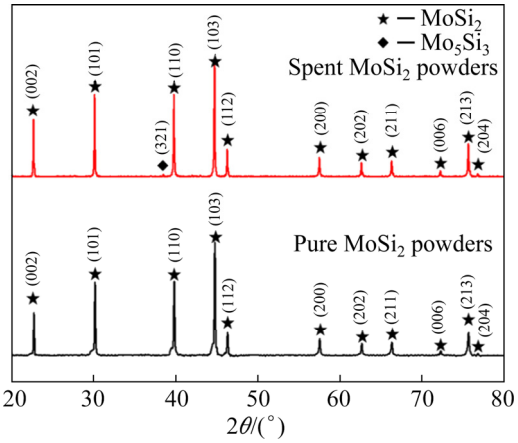

Fig. 3 XRD patterns of pure $MoSi_2$ and spent $MoSi_2$ powders

TEM image and high-resolution morphology of spent $MoSi_2$ powders are represented in Fig. 4. The interplanar spacings of the (002) and (103) planes of $MoSi_2$ are approximately 3.9231 and 2.0264 Å (Fig. 4(b)), respectively, after comparing with the standard XRD PDF card of No. 41-0612 ($MoSi_2$). In addition, a layer of amorphous phase (aluminosilicate) is observed to surround $MoSi_2$ particles. Bentonite (aluminosilicate) is added into $MoSi_2$ as the sintering additive during the preparation of $MoSi_2$-based materials [10]. However, no peak of bentonite is observed in the XRD patterns. The content of bentonite is too low (about 10 wt.%) to be detected in spent $MoSi_2$. Furthermore, the absorption coefficient of XRD is increased with increasing atomic number, the atomic number of aluminosilicates is less than the Mo−Si phase, and thus notably weak intensity is acquired by bentonite [16].

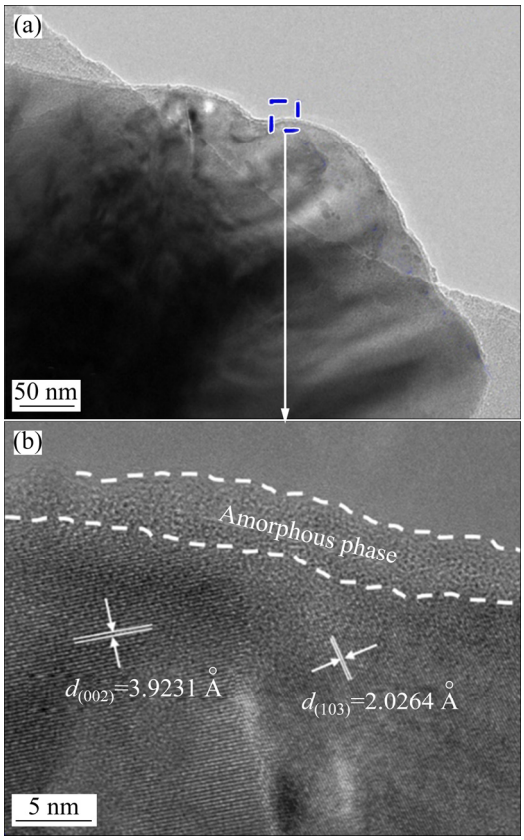

Fig. 4 TEM image (a) and high-resolution morphology (b) of spent $MoSi_2$ powders

After sintering, the XRD patterns of PM and SM coatings are provided in Fig. 5. As shown, $MoSi_2$, Mo_5Si_3, SiO_2 and $CaMoO_4$ phases appear in the two coatings. $MoSi_2$ phase is oxidized to MoO_3 and SiO_2 phases during the heating period of the sintering [17]:

$$2MoSi_2+7O_2=2MoO_3+4SiO_2 \quad (2)$$

When the sintering temperature remains unchanged at 1400 °C, the thickness of the silica layer is increased as time prolongs. The low oxygen partial pressure between $MoSi_2$ and SiO_2 layer inhibits the formation of MoO_3, causing $MoSi_2$ to be oxidized to SiO_2 and Mo_5Si_3 [18]:

$$5MoSi_2+7O_2=Mo_5Si_3+SiO_2 \quad (3)$$

In addition, the glass powders and Si also provide SiO_2 phases during oxidation. However,

MoO_3 is not found in XRD patterns since it is in the volatile state above 750 °C. Furthermore, reaction can occur between MoO_3 and CaO, making the formation of $CaMoO_4$ [19]:

$$CaO+MoO_3=CaMoO_4 \quad (4)$$

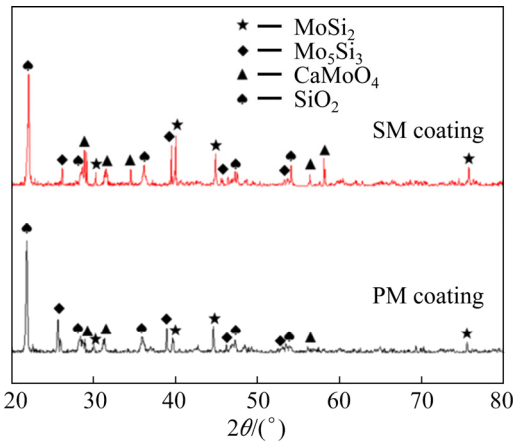

Fig. 5 XRD patterns of PM (a) and SM (b) coatings after sintering

After sintering, the surface morphologies of PM and SM coatings are represented in Fig. 6. The surfaces of PM and SM coatings are both made up of gray and white phases, which are detected to be SiO_2 and $CaMoO_4$ by EDS in Table 2, respectively, which is consistent with the XRD patterns (Fig. 5). No obvious pores are found on the surface of PM and SM coatings and this is mainly attributed to the formation of $CaMoO_4$ phase. At elevated temperatures, pores are generated in the coating by the volatilization of MoO_3 based on Eq. (2), and $CaMoO_4$, which is formed by the reaction of MoO_3 with CaO in the glass powders, can effectively reduce the content of volatile MoO_3 that penetrates into the oxide scale. According to Refs. [20,21], $CaMoO_4$ possesses excellent chemical stability, and thus it is hard to be eroded by oxygen. In addition, $CaMoO_4$ possesses a lower melting temperature (950 °C) than the sintering temperature, and it is in liquid phases at elevated temperature, which effectively promotes the densification sintering. It is also found that the amount of $CaMoO_4$ phases in SM coating is larger than that of PM coating (Figs. 6(a, b)), which is attributed to the CaO in spent $MoSi_2$ powders. However, obvious cracks can be detected on the surface of PM coating after sintering. During the cooling process, thermal stress in the coating causes the generation of cracks since a mismatch of thermal expansion coefficient

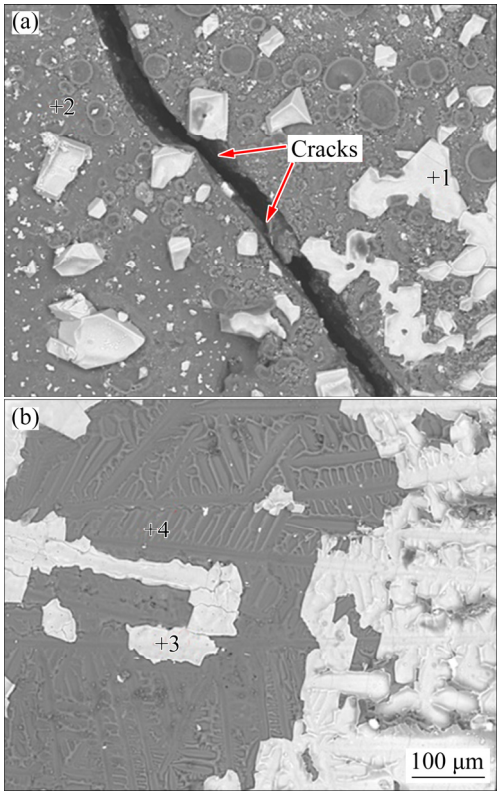

Fig. 6 Surface morphologies of PM (a) and SM (b) coatings after sintering

Table 2 Contents of Mo, Si, O and Ca by EDS in Fig. 6 (wt.%)

Point	Mo	Si	O	Ca
1	30.8	–	44.37	24.83
2	–	48.21	51.79	–
3	23.23	–	49.84	26.93
4	–	48.85	51.15	–

(CTE) exists between $MoSi_2$ (8.1×10^{-6} K^{-1}) and SiO_2 (0.6×10^{-6} K^{-1}) [21]. By contrast, no cracks are observed in SM coating, and the crack-free morphologies can be attributed to the existence of bentonite and SiO_2 phases in the spent $MoSi_2$ powders. Many reports [22−24] claim that the addition of the phases that possess low CTE can adjust the CTE value of the composites, and the content and CTE of the components in the composites controls the general CTE [25], which is given in Eq. (5):

$$\alpha_{co}=\sum_{k=1}^{n}\alpha_k w_k \quad (5)$$

where α_{co} and α_k are the CTE values of the composite coating and component k, respectively,

w_k is the mass fraction of the component k, and n is the component number. Bentonite ($1.0\times10^{-6}\,K^{-1}$) has low CTE [26], and the CTE value of spent $MoSi_2$ is calculated to be $7.39\times10^{-6}\,K^{-1}$ by Eq. (5), exhibiting that the addition of bentonite effectively reduces the CTE mismatch between the coating and oxide scale. In addition, bentonite is in the liquid phase during sintering due to its low melting temperature (1340 °C), which benefits the acceleration of the redistribution of coating powders to promote the densification of powders during sintering [27].

Figure 7 shows cross-sectional morphologies of PM and SM coatings after sintering. As shown in Figs. 7(a, e), the coatings are divided into three layers (I, II and III) after sintering, and no

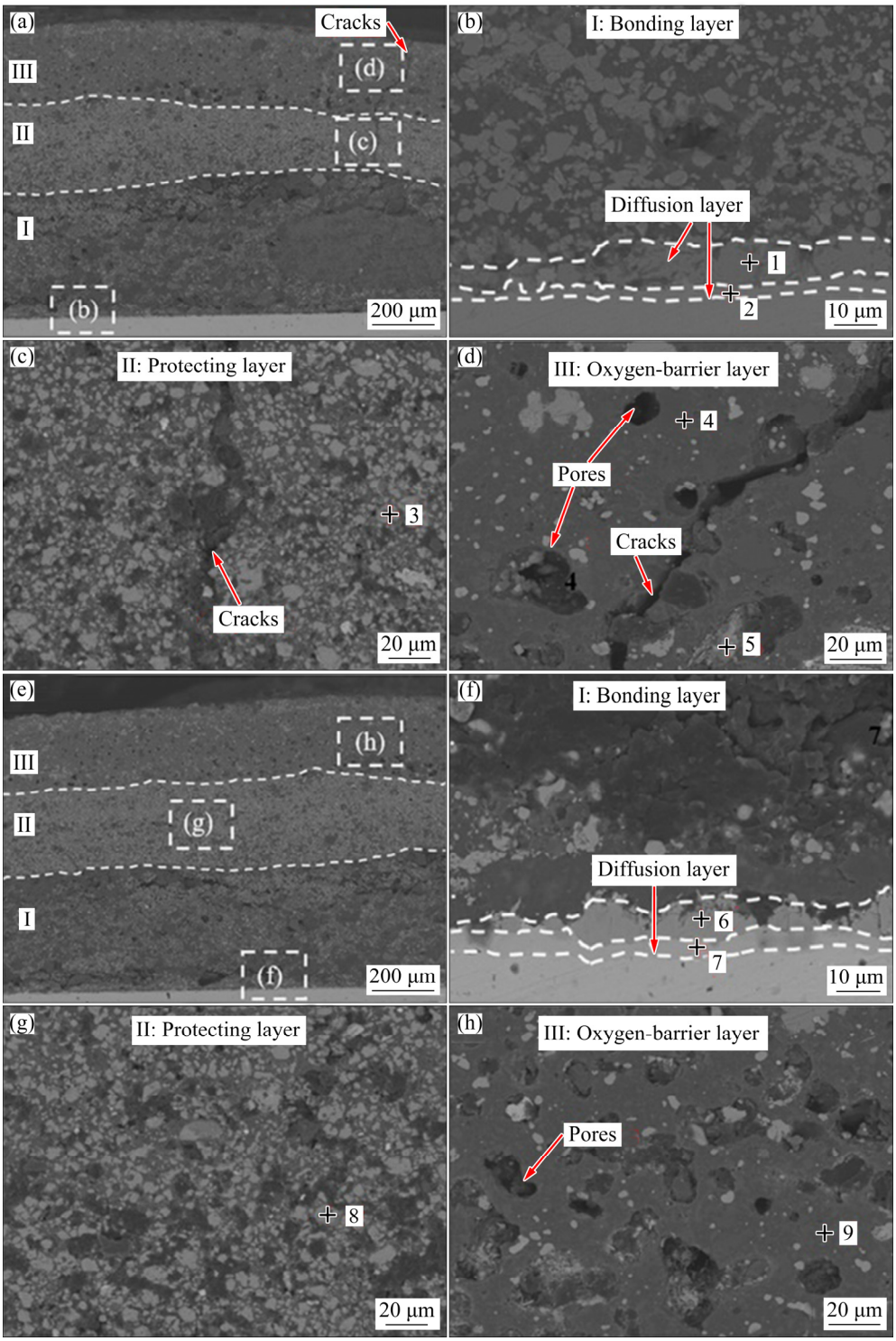

Fig. 7 Cross-sectional morphologies of PM (a−d) and SM (e−h) coatings after sintering

Table 3 Contents of Mo, Si, O and Ca by EDS in Fig. 7 (wt.%)

Point	Mo	Si	O	Ca
1	30.21	69.79	–	–
2	83.56	16.44	–	–
3	37.06	62.94	–	–
4	–	47.31	52.69	–
5	27.31	–	43.47	29.22
6	29.33	70.67	–	–
7	77.69	22.31	–	–
8	34.29	65.71	–	–
9	–	50.64	49.36	–

debonding and spalling exist between the layers, indicating that the layers in the coatings are closely bonded. Furthermore, no oxidation of Mo substrate is found in PM and SM coatings since no gaps caused by the oxidation of Mo are detected between the coating and substrate, illustrating that the substrate keeps unoxidized morphologies during the short-term sintering in air. Layer I is the bonding layer (Figs. 7(a, b)) and mainly made up of $MoSi_2$ and small amounts of Si. The formation of Mo_5Si_3 and $MoSi_2$ diffusion layers can be also found between the substrate and coating. Layer II is the protecting layer and its major composition is $MoSi_2$. Layer III is the oxygen-barrier layer and consists of SiO_2 and $CaMoO_4$ phases. However, a slight longitudinal crack appears in the Layer II and Layer III of the PM coating due to the CTE mismatch between the $MoSi_2$ coating and oxygen-barrier layer. The cracks may provide diffusion path for O_2, which will decrease the oxidation resistance of the coating. Although the bonding layer and protecting layer are relatively dense without any large-sized cracks, pores can be also observed in the oxide scale of the PM coating. During high-temperature sintering in air, Reaction (2) occurs in the $MoSi_2$-based coating, and $MoSi_2$ is oxidized to volatile MoO_3. Layer III is close to the oxygen and it first undergoes violent oxidation in air to form SiO_2 oxide scale to block the O_2 diffusion, but pores are also generated by the volatilization of MoO_3. By comparison, no direct contact exists between Layer I−II and the air, and the oxide scale in Layer III also provides corresponding protective effect to inhibit the oxidation. Therefore, rare oxidation reactions happen in the protecting layer and bonding layer, leading to relatively fewer pores found in the two layers.

In comparison with PM coating, although SM coating (Fig. 7(h)) possesses rare amounts of pores in Layer III (oxide scale), it exhibits relatively crack-free coating morphologies after high-temperature sintering. Furthermore, $MoSi_2$ and Mo_5Si_3 diffusion layers are found between the coating and Mo substrate without debonding or gaps, showing good metallurgical bonding after sintering. At high temperatures, Si has high activity and it diffuses into the Mo substrate to form $MoSi_2$ layer. In addition, Si atoms in the $MoSi_2$ layer also diffuse into Mo, which causes the generation of Mo_5Si_3 diffusion layer. It is shown that the diffusion layer can strengthen the bonding via improving the metallurgical bonding between coating and substrate [28] since the mutual diffusion between atoms can promote the formation of a firmly metallurgical interface between coating and substrate at high temperature. Therefore, the formation of the diffusion layers generated by the mutual diffusion of Si and Mo plays an important role in the metallurgical bonding of the coating and substrate, which effectively prevents the spalling and debonding of the coating, and thus the bonding between coating and substrate is strengthened.

3.2 Oxidation behavior of PM and SM coatings at 1500 °C

The XRD patterns of PM and SM coatings after oxidation of 20 h at 1500 °C are shown in Fig. 8. Small amounts of $MoSi_2$ phase can be still detected in the surface of PM coating after oxidation while only SiO_2 and $CaMoO_4$ phases

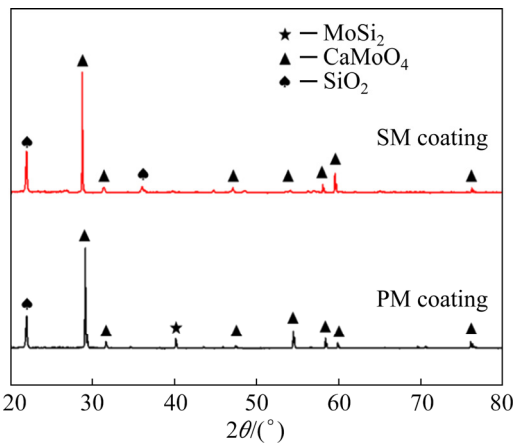

Fig. 8 XRD patterns of PM and SM coatings after oxidation at 1500 °C for 20 h

exist in the surface of SM coating. Compared with the coatings before oxidation, the amounts of $MoSi_2$ phases sharply decrease since $MoSi_2$ phases in the coating surface react with O_2 to form SiO_2 during oxidation at elevated temperature by Eq. (3) [19].

Figure 9 presents the surface morphologies of PM and SM coatings after oxidation of 20 h at 1500 °C. According to Figs. 9(a, b) and Table 4, the gray oxide scale (SiO_2) of PM coating is smooth with some white phase ($CaMoO_4$) occupying on the surface, indicating that large amounts of SiO_2 are generated during oxidation. As reported [29], silica can improve the anti-oxidation properties of the coating because softened SiO_2 can fill the micro-cracks or pores in a high-temperature environment, which blocks the diffusion path of oxygen. Furthermore, SiO_2 possesses a low oxygen diffusion coefficient (4.4×10^{-15} m^2/s) at high temperature [30] and it serves as the oxygen barrier to inhibit further oxidation in the coating. Thus, no obvious cracks can be found in the PM coating after long-term oxidation due to the self-healing effect of silica. However, some large-sized pores (about 20 μm), which are caused by volatile MoO_3 during high-temperature oxidation, are observed on the surface of the oxide scale of PM coating, and they are beneficial to the high-temperature diffusion of O_2. As shown in Figs. 9(c, d), although some pores are found in the silica oxide scale of SM coating, the size of the pores is much smaller (about 6 μm), and the oxide scale is dense and complete with even distribution of white $CaMoO_4$ phase on the surface. Thus, SM coating shows improved oxidation resistance than PM coating.

The mass gains of PM and SM coatings during oxidation at 1500 °C for 0−20 h are shown in Fig. 10(a). Although rapid mass gains of the two coatings occur during initial oxidation (0−5 h), the rate of the mass gain decreases as the oxidation time prolongs (5−20 h). After oxidation of 20 h, the mass gains of PM and SM coatings reach the maximum values of 9.21 and 6.28 mg/cm^2, and the oxidation rates decrease to the minimum values of 0.46 and 0.31 $mg/(h\cdot cm^2)$, respectively. According to Fig. 11, which presents the standard Gibbs free energy change of Reactions (2)−(4) from 0 to 2000 °C, Reactions (2) and (3) have relatively low free energy among the oxidation reactions, exhibiting that SiO_2 is preferentially formed by the oxidation of $MoSi_2$. During the rapid mass change stage (0−5 h), or Stage I, the formation of SiO_2 causes the rapid mass gain of the coating. When the oxidation time increases (5−20 h, Stage II), the reaction rate of $MoSi_2$ with O_2 decreases because of

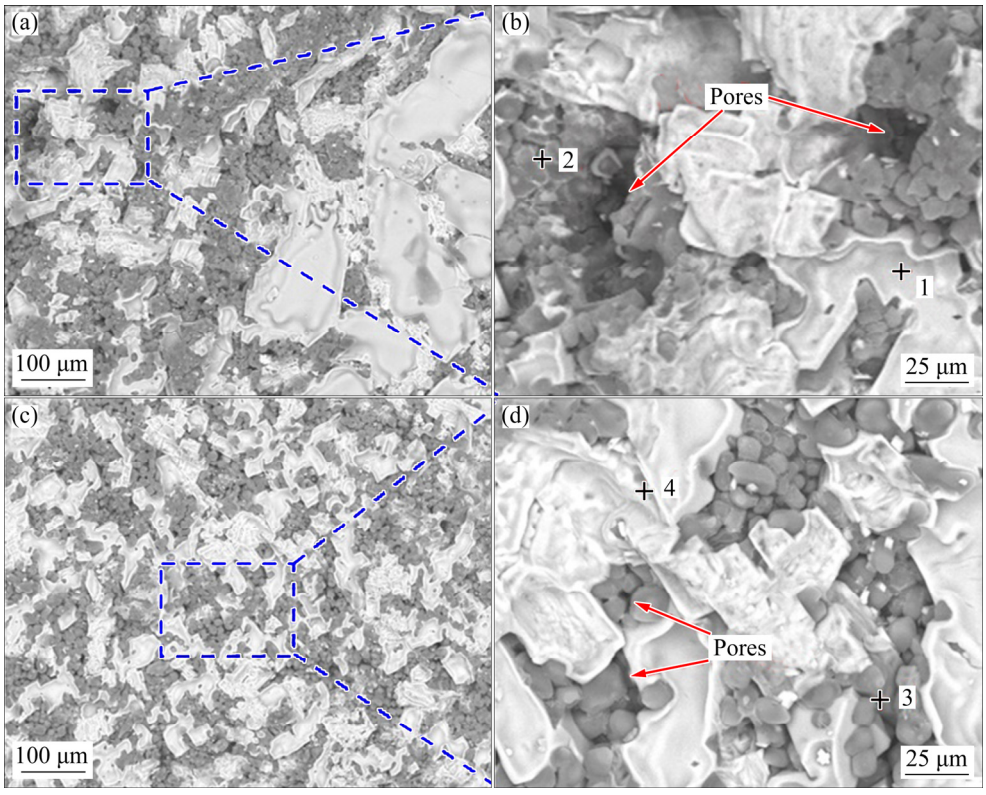

Fig. 9 Surface morphologies of PM (a, b) and SM (c, d) coatings after oxidation at 1500 °C for 20 h

Table 4 Contents of Mo, Si, O and Ca by EDS in Fig. 9 (wt.%)

Point	Mo	Si	O	Ca
1	30.82	–	44.46	24.72
2	–	51.83	48.17	–
3	–	48.95	51.05	–
4	37.32	–	33.64	29.04

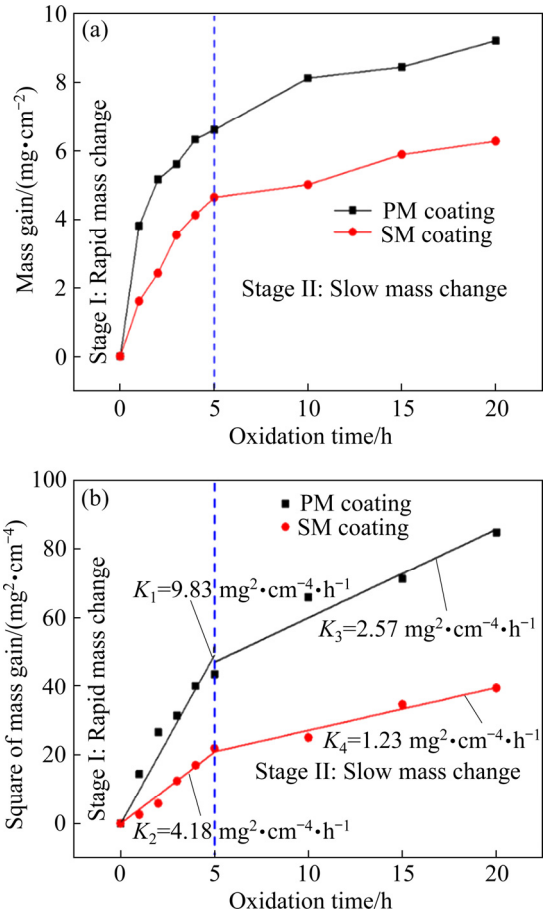

Fig. 10 Mass gain (a) and corresponding fitting curves of oxidation time versus square of mass gain (b) of PM and SM coatings after oxidation at 1500 °C for 0−20 h

the generated SiO_2 layer that possesses low oxygen diffusion coefficient, thus making the mass gain of the coatings slow down. As shown in Fig. 10(b), which presents the fitting curves of the mass gain of PM and SM coating after oxidation of 0−20 h at 1500 °C, the relationship between oxidation time and square of mass gain approximately obeys a linear relationship in Stages I and II. The oxidation rate constants (K) of PM and SM coatings are calculated to be 9.83 and 4.18 $mg^2 \cdot cm^{-4} \cdot h^{-1}$ in Stage I (rapid mass change), and 2.57 and 1.23 $mg^2 \cdot cm^{-4} \cdot h^{-1}$ in Stage II (slow mass change),

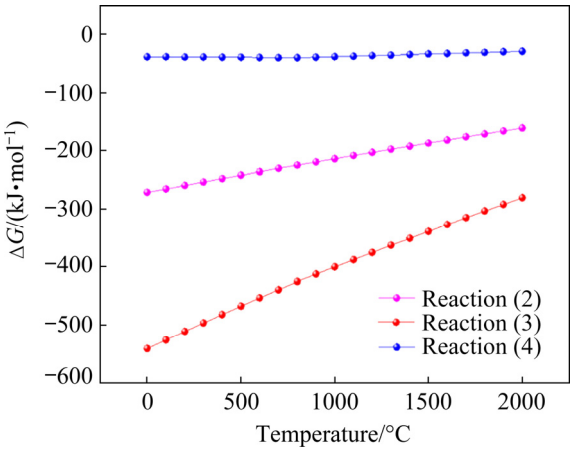

Fig. 11 Standard Gibbs free energy change of Reactions (2)−(4) from 0 to 2000 °C

respectively. Compared with PM coating, SM coating exhibits lower mass gain and oxidation rate constant at 1500 °C because of the relatively crack-free and dense morphologies after sintering, which is beneficial to inhibiting the high-temperature diffusion of O_2. Therefore, SM coating shows better anti-oxidation properties.

Cross-sectional morphologies of PM and SM coatings after oxidation at 1500 °C for 20 h are shown in Fig. 12. In Figs. 12(a−c), PM coating still maintains layered structure after 20 h oxidation. Layer I is mainly made up of $MoSi_2$, and Layer II consists of $MoSi_2$ and SiO_2 that are formed during oxidation. Layer III is the oxide scale (541 μm), the composition of which is SiO_2 and $CaMoO_4$ phases, and some pores are found in the oxide scale as well. After oxidation of 20 h at 1500 °C, an obvious diffusion layer is detected in the PM coating. According to the EDS analysis (Fig. 5), the diffusion layer mainly consists of the $MoSi_2$ layer and Mo_5Si_3 layer because Si continuously reacts with Mo at elevated temperatures. The diffusion coefficient of Si and reaction time influence the diffusion layer thickness in high-temperature environment. Compared with the sintering process, the temperature of the oxidation is higher and it makes the diffusion coefficient of Si increase. Furthermore, the increasing oxidation time causes the thickening of the diffusion layer as well. As shown in Figs. 12(d−f), layered structure can be also observed in the SM coating, which has similar chemical composition in Layers I, II and III of PM coating. Although some pores exist in the oxide scale, no debonding or obvious cracks can be

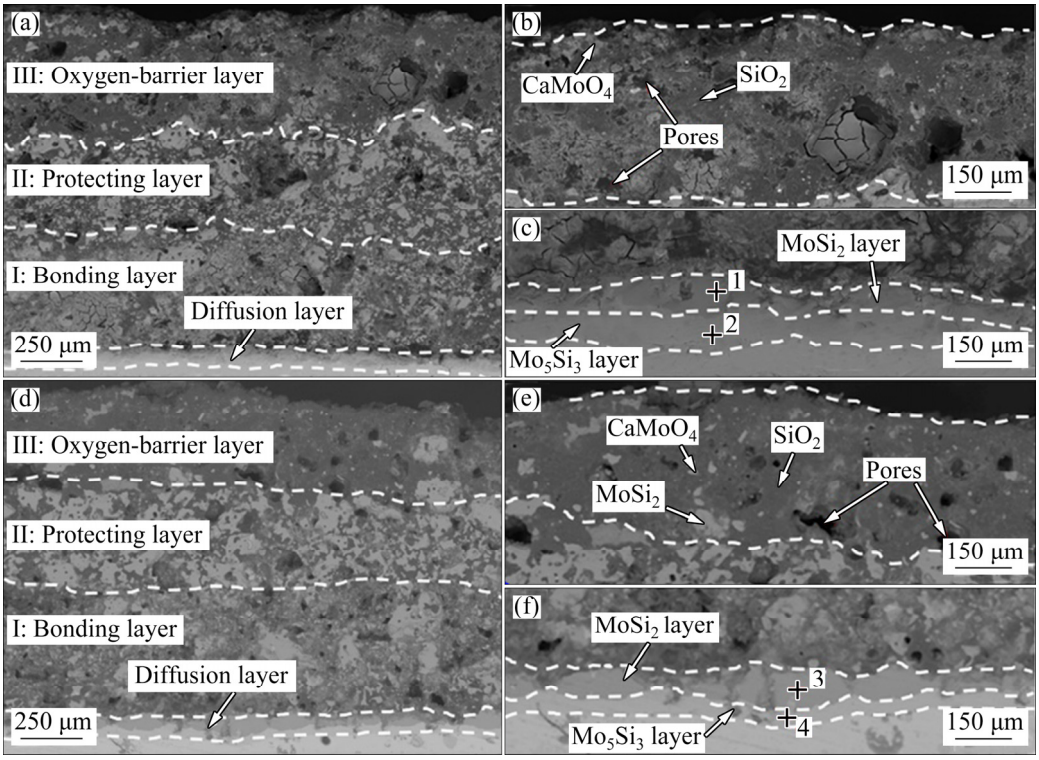

Fig. 12 Cross-sectional morphologies of PM (a−c) and SM (d−f) coatings after oxidation at 1500 °C for 20 h

Table 5 Contents of Mo and Si by EDS in Fig. 12 (wt.%)

Point	Mo	Si
1	64.82	35.18
2	85.41	14.59
3	64.78	35.22
4	85.51	29.04

detected after oxidation of 20 h. Compared with PM coating, SM coating has relatively crack-free and dense morphologies with a thinner oxide scale (423 μm), showing less consumption of the coating with improved anti-oxidation properties.

Figure 13 represents the schematic diagram of the sintering and oxidation mechanism of SM coating on Mo substrate. During sintering, large numbers of Si atoms in Layer I diffuse into Mo substrate to form the $MoSi_2$ layer. As the sintering time increases, Si atoms diffuse into Mo to form diffusion layers and the bonding layer is formed to enhance the metallurgical bonding between the coating and substrate. Layer II, which possesses the highest content of the $MoSi_2$ phase, is the major structure of the coating system and it acts as the protecting layer to safeguard the Mo substrate. These $MoSi_2$ phases are covered by bentonite with low melting temperature and good oxidation resistance, which is conducive to improve the compactness of the coating and anti-oxidation properties during sintering. Layer III plays the most important role in preventing the diffusion of oxygen. During sintering, the $MoSi_2$ and Si in the coating are oxidized to SiO_2, which is the main phase of the oxygen-barrier layer. The glass powders also provide plenty of SiO_2 phases for Layer III. SiO_2 has a low oxygen diffusion coefficient and it can block the oxygen diffusion channel to improve the oxidation resistance of the coating. In addition, the CaO phase in the glass powders reacts with volatile MoO_3 to form $CaMoO_4$ that has good chemical stability, inhibiting the formation of pores in the coating. As the oxidation time prolongs and the temperature rises (1500 °C), the Mo_5Si_3 diffusion layer is thickened by the diffusion of Si. Furthermore, the thickness of the oxide scale increases due to the oxidation of the $MoSi_2$ phase in Layer III. After high-temperature oxidation, except for some pores in the oxide scale, no obvious defects such as debonding and spalling can be detected in Layers I, II and III, exhibiting that SM coating possesses good anti-oxidation properties at elevated temperature.

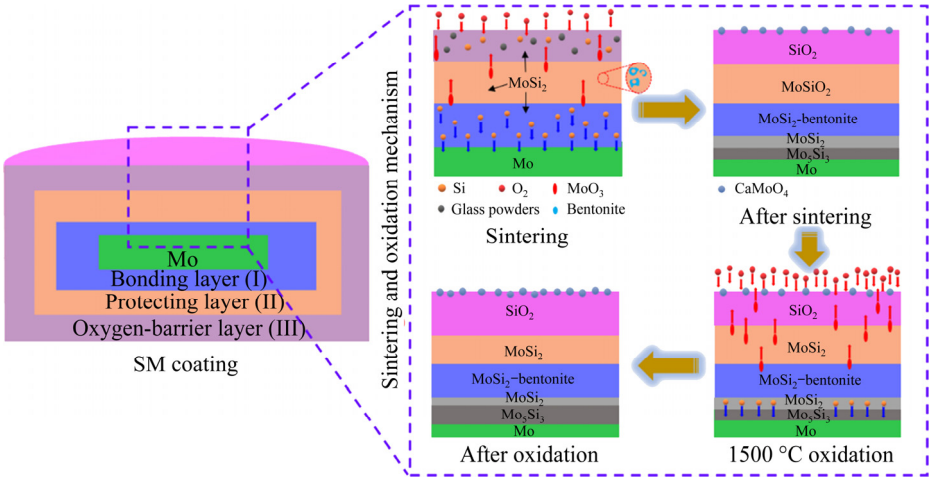

Fig. 13 Schematic diagram of sintering and oxidation mechanism of SM coating on Mo substrate

4 Conclusions

(1) Spent $MoSi_2$ is successfully recycled to prepare the multilayer $MoSi_2$-based anti-oxidation coating on Mo substrates by slurry painting. $MoSi_2$, Mo_5Si_3, SiO_2 and $CaMoO_4$ phases are detected in PM and SM coatings after sintering, and the formation of pores caused by volatile MoO_3 is inhibited by the reaction of MoO_3 with CaO in the glass powders. Obvious cracks are formed in the PM coating after short-term sintering while the SM coating is crack-free and complete without debonding or gaps.

(2) Although no obvious cracks are detected in the surface of PM coating after oxidation of 20 h, large-sized pores can be still observed in the silica layer while a relatively dense and continuous silica layer with rare amounts of pores is generated on SM coating. These large-sized pores provide a diffusion path for oxygen to react with $MoSi_2$, causing rapid mass gain of PM coating. After oxidation of 20 h at 1500 °C, the mass gain of SM coating is only 6.28 mg/cm^2, which is lower than that of PM coating (9.21 mg/cm^2). $MoSi_2$ and Mo_5Si_3 diffusion layers are generated in SM coatings during oxidation and the oxide scale of SM coating is thinner than PM coating, exhibiting less coating consumption with better anti-oxidation properties at high temperatures.

Acknowledgments

This research was financially supported by the National Natural Science Foundation of China (Nos. 51874305, 51972338) and Graduate Research and Innovation Projects of Jiangsu Province, China (No. KYCX21_22413). We are grateful to the Advanced Analysis & Computation Center of China University of Mining and Technology.

References

[1] LI Wei, FAN Jing-lian, FAN Yan, XIAO Lai-rong, CHENG Hui-chao. $MoSi_2$/(Mo,Ti)Si_2 dual-phase composite coating for oxidation protection of molybdenum alloy [J]. Journal of Alloys and Compounds, 2018, 740: 711−718.

[2] ZHOU Yu-cheng, GAO Yi-min, WEI Shi-zhong, PAN Kun-ming, HU Ya-jie. Preparation and characterization of Mo/Al_2O_3 composites [J]. International Journal of Refractory Metals and Hard Materials, 2016, 54: 186−195.

[3] CAO Yuan-kui, LIU Yong, LIU Bin, ZHANG Wei-dong, WANG Jia-wen, DU Meng. Effects of Al and Mo on high temperature oxidation behavior of refractory high entropy alloys [J]. Transactions of Nonferrous Metals Society of China, 2019, 29(7): 1476−1483.

[4] VASUDEVAN A K, PETROVIC J J. A comparative overview of molybdenum disilicide composites [J]. Materials Science and Engineering A, 1992, 155(1/2): 1−17.

[5] ZHAI Da-jun, FENG Ke-qin. Preparation of micro/nano-structured ceramic coatings on Ti6Al4V alloy by plasma electrolytic oxidation process [J]. Transactions of Nonferrous Metals Society of China, 2019, 29(12): 2546−2555.

[6] ZOU Ke, ZOU Jian-peng, DENG Chun-ming, LIU Min, LIU Xue-zhang, ZHAO Rui-min, LI Shun-hua, ZHU Ren-bo, GAO Di. Preparation and properties of supersonic atmospheric plasma sprayed TiB_2−SiC coating [J]. Transactions of Nonferrous Metals Society of China, 2021, 31(1): 243−254.

[7] XU Jiang-guang, ZHANG Hou-an, JIANG Guo-jian, ZHANG Bao-lin, LI Wen-lan. SiC whisker reinforced $MoSi_2$ composite prepared by spark plasma sintering from COSHS-ed powder [J]. Transactions of Nonferrous Metals Society of China, 2006, 16(S2): s504−s507.

[8] REN Xuan-ru, LV Jun-shuai, HU Yu-wen, SUN Ke, MA Can, CHU Hong-ao, WANG Wei-guang, XU Lei-hua, LI Zi-yu, FENG Pei-zhong. Influence of $MoSi_2$ on oxidation protective ability of TaB_2−SiC coating in oxygen-containing environments within a broad temperature range [J]. Journal

of Advanced Ceramics, 2020, 9: 703−715.
[9] ZHANG Yu-lei, LI He-jun, HU Zhi-xiong, LI Ke-zhi, ZHANG Lei-lei. C/SiC/$MoSi_2$−SiC−Si multilayer coating for oxidation protection of carbon/carbon composites [J]. Transactions of Nonferrous Metals Society of China, 2013, 23(7): 2118−2122.
[10] BIZZARRI C, LINDER B, LINDSKOG N. Molybdenum disilicide heating elements [J]. American Ceramic Society Bulletin, 1989, 68: 1834−1835.
[11] OLIVETTI E A, CULLEN J M. Toward a sustainable materials system [J]. Science, 2018, 360: 1396−1398.
[12] FU Qian-gang, LI He-jun, WANG Yong-jie, LI Ke-zhi, SHI Xiao-hong. B_2O_3 modified SiC–$MoSi_2$ oxidation resistant coating for carbon/carbon composites by a two-step pack cementation [J]. Corrosion Science, 2009, 51(10): 2450−2454.
[13] LIU Fei, LI He-jun, GU Sheng-yue, YAO Xi-yuan, FU Qian-gang. Spraying power influence on microstructure and bonding strength of $ZrSi_2$ coating for SiC coated carbon/carbon composites [J]. Ceramics International, 2018, 44(6): 6619−6625.
[14] YAN Jiang, YE Chao-chao, RU Hong-qiang, WANG Wei, ZHANG Cui-ping, YUE Xin-yan. Oxidation protective $MoSi_2$−SiC−Si coating for graphite materials prepared by slurry dipping and vapor silicon infiltration [J]. Ceramics International, 2018, 44(5): 5171−5178.
[15] ZHU Lu, REN Xuan-ru, WANG Xiao-hong, KANG Xue-qin, ZHENG Rui-xin, FENG Pei-zhong. Microstructure and high-temperature oxidation resistance of $MoSi_2$−ZrO_2 composite coatings for niobium substrate [J]. Journal of the European Ceramic Society, 2021, 41(2): 1197−1210.
[16] DEEVI S C, DEEVI S. In-situ synthesis of $MoSi_2$−Al_2O_3 composite by a thermite reaction [J]. Scripta Metallurgica et Materialia, 1995, 33: 415−420.
[17] GUO Shu-qi, MIZUGUCHI T, IKEGAMI M, KAGAWA Y. Oxidation behavior of ZrB_2−$MoSi_2$−SiC composites in air at 1500 °C [J]. Ceramics International, 2011, 37(2): 585−591.
[18] ZHANG Wu-zhuang, ZENG Yi, GBOLOGAH L, XIONG Xiang, HUANG Bai-yun. Preparation and oxidation property of ZrB_2−$MoSi_2$/SiC coating on carbon/carbon composites [J]. Ceramics International, 2011, 21(7): 1538−1544.
[19] INGEMARSSON L, HALVARSSON M, ENGKVIST J, JONSSON T, HELLSTRÖM K, JOHANSSON L G, SVENSSON J E. Oxidation behavior of a Mo(Si,Al)$_2$-based composite at 300−1000 °C [J]. Intermetallics, 2010, 18: 633−640.
[20] ANSARI A A, PARCHUR A K, ALAM M, AZZEER A. Structural and photoluminescence properties of Tb-doped $CaMoO_4$ nanoparticles with sequential surface coatings [J]. Materials Chemistry and Physics, 2014, 147: 715−721.
[21] MIKHAYLOVSKAYA Z A, ABRAHAMS I, PETROVA S A, BUYANOVA E, TARAKINA N V, PIANKOVA D V, MOROZOVA M V. Structural, photocatalytic and electro-conductive properties of bismuth-substituted $CaMoO_4$ [J]. Journal of Solid State Chemistry, 2020, 291: 121627.
[22] ZHANG Hou-an, GU Si-yong. Preparation and oxidation behavior of $MoSi_2$–$CrSi_2$–Si_3N_4 composite coating on Mo substrate [J]. International Journal of Refractory Metals and Hard Materials, 2013, 41: 128−132.
[23] FU Qian-gang, ZHANG Jia-ping, ZHANG Zheng-zhong, LI He-jun, SUN Can. SiC–$MoSi_2$/ZrO_2–$MoSi_2$ coating to protect C/C composites against oxidation [J]. Transactions of Nonferrous Metals Society of China, 2013, 23(7): 2113−2117.
[24] YOON J, KIM G, BYUN J, LEE J, PAIK Y, KIM J. Formation of $MoSi_2$−Si_3N_4 composite coating by reactive diffusion of Si on Mo substrate pretreated by ammonia nitridation [J]. Scripta Materialia, 2002, 47: 249−253.
[25] FAHMY A A, RAGAI A N. Thermal-expansion behavior of two-phase solids [J], Journal of Applied Physical, 1971, 41: 5108−5111.
[26] JONNY R, BÖRGESSON L, CHIJIMATSU M, FU S, SON T N. Coupled thermo-hydro-mechanical analysis of a heater test in fractured rock and bentonite at Kamaishi Mine—Comparison of field results to predictions of four finite element codes [J]. International Journal of Rock Mechanics and Mining Sciences, 2001, 38: 129−142.
[27] ADAMIS Z. Bentonite, kaolin, and selected clay minerals [M]. Geneva: World Health Organization, 2005.
[28] HUANG Xiao-shan, YAN Long-ge, ZHANG Xin-fang. Electromigration-enhanced atomic diffusion to improve coating interface bonding [J]. Scripta Materialia, 2021, 202: 114017.
[29] HE Zi-bo, LI He-jun, SHI Xiao-hong, FU Qian-gang, WU Heng. Formation mechanism and oxidation behavior of $MoSi_2$−SiC protective coating prepared by chemical vapor infiltration/reaction [J]. Transactions of Nonferrous Metals Society of China, 2013, 23(7): 2100−2106.
[30] SUCOV E W. Diffusion of oxygen in vitreous silica [J]. Journal of the American Ceramic Society, 2006, 46: 14−20.

钼基体表面二硅化钼涂层的制备及其高温抗氧化性能

朱 路[1,2]，陈 鹏[1]，蔡子明[1]，冯培忠[1]，康学勤[1]，Farid AKHTAR[3]，王晓虹[1]

1. 中国矿业大学 材料与物理学院，徐州 221116；2. 中国矿业大学 化工学院，徐州 221116；
3. Division of Materials Science, Luleå University of Technology, Luleå 97187, Sweden

摘 要：以工业废弃硅化钼棒为原料，采用浆料涂刷法在钼表面制备 $MoSi_2$ 基抗氧化涂层。研究涂层的显微组织、相组成及在 1500 ℃的高温氧化行为。结果表明，以废弃硅化钼棒和纯 $MoSi_2$ 粉末为原料制备的涂层和基体之间形成明显的连接层。纯 $MoSi_2$ 制备的涂层(PM)在烧结后出现少量裂纹，而以废弃硅钼棒为原料制备的涂层(SM)在烧结后没有裂纹。1500 ℃氧化后，PM 涂层的氧化膜存在较大尺寸的孔隙，而 SM 涂层表面氧化膜相对更完整和致密，且在氧化过程中质量增加更少，表现出更好的抗氧化性能。

关键词：再利用；废弃硅化钼棒；浆料涂刷；抗氧化性能；钼基体

(Edited by Bing YANG)